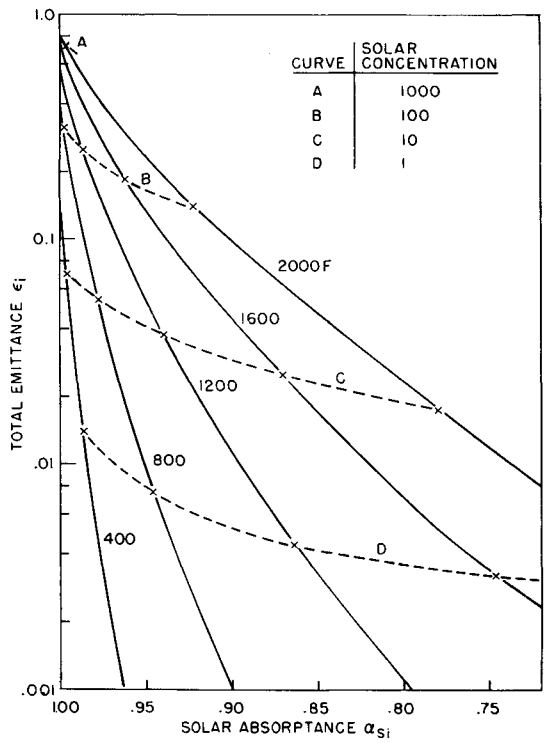

Fig. 3 Solar absorptance and total emittance of ideal absorber.

surface to that for an ideal selective absorber under the same conditions

$$\phi = \frac{q}{q_i} = \frac{\alpha_s H_s - \epsilon\sigma T^4}{\alpha_{si} H_s - \epsilon_i \sigma T^4} \qquad \alpha_{si} \neq 1 \qquad \epsilon_i \neq 0 \qquad (3)$$

where the subscript i denotes the ideal absorber. The values of α_{si} and ϵ_i depend on the cutoff wavelength (i.e. the surface temperature and solar concentration) and are plotted in Fig. 3.

Knowing the radiation properties of a material, one can plot ϕ vs T with solar energy concentration as the parameter. The solid curves in Fig. 4 show ϕ for one of the better space-stable high-temperature solar absorbers available today.[1–5] The dashed curves in Fig. 4 are for a blackbody that would be an excellent absorber for high solar energy concentrations. Also, one can see that the advantage of a low emittance value is not critical for certain conditions, because the blackbody ($\alpha_s/\epsilon = 1.0$) would give a higher ϕ than the selective surface ($\alpha_s/\epsilon = 7.0$) for a considerable range of the conditions. In general, a selective absorber has advantages over a blackbody at the lower solar concentrations and higher temperatures.

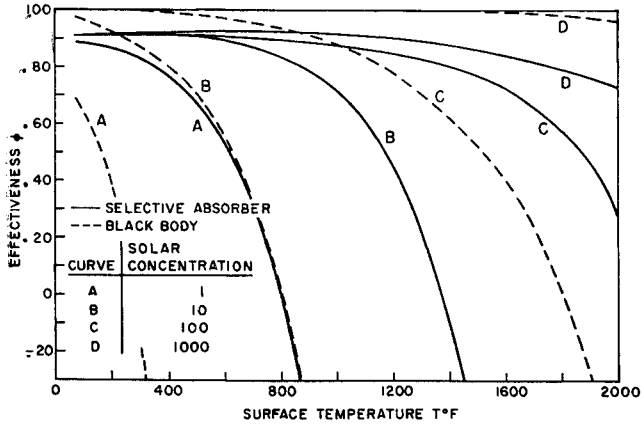

Fig. 4. Effectiveness of an available selective absorber and a blackbody.

Negative effectiveness means more energy is radiated away than absorbed; therefore the surface is no longer a solar absorber but is classified as a radiator.

References

[1] Schmidt, R. N. and Janssen, J. E., "Selective coatings for vacuum stable high temperature solar absorbers," Symposium on Thermal Radiation of Solids (March 1964).

[2] Schmidt, R. N., Park, K. C., Torborg, R. H., and Janssen, J. E., "High temperature solar absorber coatings, Part I," Air Force Material Lab., Air Force Systems Command, RTD-TDR-63-579 (November 1963).

[3] Schmidt, R. N., Park, K. C., and Janssen, J. E., "High temperature solar absorber coatings, Part II," Air Force Material Lab., Research and Technology Div., Air Force Systems Command, ML-TDR-64-558 (September 1964).

[4] Butler, C. P., Jenkins, R. J., and Parker, W. J., "Solar absorptance and total hemispherical emittance of surfaces for solar energy collection," Directorate of Material and Processes, Aeronautical Systems Div., Air Force Systems Command ASD-TR-61-558 (July 1962).

[5] Edwards, D. K., Gier, J. T., Nelson, K. E., and Roddick, R. D., "Spectral and directional thermal radiation characteristics of selective surfaces for solar collectors," Solar Energy **VI**, 1 (January-March 1962).

Variable-Mass Vehicle Limit-Cycle Propellant Consumption

DONALD FREDERICK REEVES*
The Marquardt Corporation, Van Nuys, Calif.

Nomenclature

a = Flt_0, ft-lb-sec
b = I_{x_1}, slug-ft^2
c = $2Ft_0 l_1^2/gI_{sp}$, slug-ft^2
F = thrust, lb
I_t = specific impulse, sec
I_{sp} = minimum impulse increment per engine, lb-sec
I_x = vehicle moment of inertia, slug-ft^2
I_{x_1} = initial moment of inertia, slug-ft^2
l = moment arm of coupled motors, ft
l_1 = propellant tank distance from axis, ft
t_0 = pulse width, sec
$\bar{\dot{\theta}}$ = average angular rate, rad/sec
θ_r = angular limit, rad
$\dot{\omega}$ = propellant flow rate per rocket motor, lb/sec

THE analytic procedures used for the study of attitude control and stabilization usually assume that the mass of the orbiting vehicle remains constant during the control period. However, any vehicle that has a sustained operational life will have a bounded propellant mass fraction. Near the end of operation, the mass and principal moments of inertia will be reduced, thus altering the dynamic characteristics of the vehicle. Regardless of the type of active stabilization used, this change in vehicle dynamics will occur. In the particular system under consideration, the expulsion of propellants during operation of the reaction control system will reduce the vehicle mass. The analysis presented in this paper shows the effect of variable mass and moments of inertia and compares the results with the case of a constant mass system.

During the fine control mode of operation, it was shown by Reeves, Boardman, and Baumann[1] that the vehicle will oscil-

Presented as Preprint 2704-62 at the ARS 17th Annual Meeting and Space Flight Exposition, Los Angeles, Calif., November 13–18, 1962; revision received July 14, 1964.

* Member of the Advanced Technical Staff. Member AIAA.

late between the required angular limits at a constant frequency and thus will have a constant propellant consumption. This cycling or limit cycle is caused by firing the reaction motors for a prescribed time at each angular limit. Neglecting time delays, thrust inaccuracies, and disturbing torques, the dynamic characteristics of the vehicle can be determined.[1] These effects may be extremely significant depending upon the operating conditions of the vehicle but have been omitted for the purpose of allowing a linear solution of the problem. This derivation results in the following equations for a constant-mass vehicle having two pairs of coupled rocket motors located symmetrically about the principal axis under consideration:

Frequency of Oscillation

$$f_1 = \Delta\dot{\theta}_0/12\theta_r \tag{1}$$

Angular Rate Increment per Pulse

$$\Delta\dot{\theta}_0 = I_{sp}\dot{\omega}lt_0/I_x \tag{2}$$

Average Propellant Consumption

$$\bar{\dot{\omega}} = I_t^2 l/3\theta_r I_{sp} I_x \tag{3}$$

These relations are useful in the determination of attitude-control propellant requirements for large vehicles where the total propellant mass is a small fraction of the total mass. However, as the operational period is lengthened or the vehicle mass reduced, an error results from the assumption of constant mass.

In the case of a variable-mass system, the frequency of oscillation will increase with time, as will the average mission propellant consumption. In the following derivation, it has been assumed that the propellant tanks are located at a fixed distance from the principal axis and that the propellant expulsion loss is the only source of mass variation. The moment of inertia of the vehicle after N pulses is

$$I_x = I_{x_1} - Nc \tag{4}$$

The angular rate increment imparted during the Nth pulse is

$$\Delta\dot{\theta}_N = a/[b-(N-1)c] \tag{5}$$

The frequency of oscillation after N pulses is

$$f_1 = a/12\theta_r(b-Nc) \tag{6}$$

The average time of one complete cycle is

$$t_1 = 4\theta_r/\bar{\dot{\theta}} \tag{7}$$

The average period determined in Ref. 1 is $12\theta_r/\Delta\dot{\theta}$. Assuming that the angular rate presented in Eq. (5) changes every second pulse, the period becomes

$$t_n = 12\theta_r/\Delta\dot{\theta}_{2n} \tag{8}$$

The total time before the Nth pulse is fired is

$$\begin{aligned} T = \Sigma t_n &= \sum_{n=0}^{N/2} \frac{12\theta_r(b-2nc)}{a} \\ &= \frac{6\theta_r bN}{a} - \left(\frac{24\theta_r c}{a}\right)\sum_{n=0}^{N/2} n \\ &= 6\theta_r bN/a - (24\theta_r\, c/a)\,(N^2/8 + N/4) \end{aligned} \tag{9}$$

Rearranging as a quadratic in N,

$$T = -3\theta_r\, cN^2/a + (b-c)\, 6\theta_r\, N/a \tag{10}$$

The total propellant used up to this time T is

$$W_p = 2FNt_0/I_{sp} \tag{11}$$

By combining Eqs. (10) and (11), the total propellant required for a given control period can be determined:

$$\begin{aligned} W_p &= 2Ft_0 a/3\theta_r c I_{sp}\,[3\theta_r\,(b-c)/a - \\ &\qquad \{9\,[\theta_r\,(b-c)/a]^2 - 3\theta_r cT/a\}^{1/2}] \\ &= (2Ft_0/I_{sp})[(b/c-1) - \{(b/c-1)^2 - aT/3\theta_r c\}^{1/2}] \end{aligned} \tag{12}$$

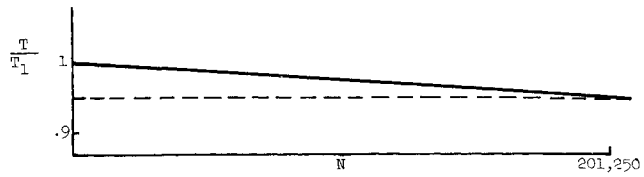

Fig. 1 Ratio of operation times vs number of pulses.

The greater root is not used in the solution, since it represents a time subsequent to depletion of the propellant.

For a fixed mass system, the total time required for N pulses is

$$T_1 = 6\theta_r bN/a \tag{13}$$

Thus, the ratio of times for the fixed mass and variable mass systems is

$$T/T_1 = 1 - c(1 + n/2)/b \tag{14}$$

The propellant required over the period T for a fixed mass system assumption is

$$W_{p_1} = I_t^2 l\; T/3\theta_r I_{sp} I_x \tag{15}$$

and the ratio of propellants for the variable and fixed mass system assumptions over the same period T is

$$\begin{aligned} W_p/W_{p_1} = 2b/cT\,[3\theta_r\,(b-c)/a - \\ \{9\,[\theta_r(b-c)/a]^2 - 3\theta_r cT/a\}^{1/2}] \end{aligned} \tag{16}$$

In order to illustrate the application of this theory, a vehicle having the following characteristics has been assumed: $\theta_r = 0.05$ rad, $F = 5$ lb, $l = 5$ ft, $t_0 = 0.01$ sec, $a = 0.25$ ft-lb-sec, $b = 100$ slug-ft^2, $l_1 = 2$ ft, $I_{sp} = 250$ sec, and $c = 0.0000496$ slug-ft^2.

Assuming that the propellant accounts for 10 slug-ft^2, which is equivalent to $W_p = 80.5$ lb at a displacement l_1 of 2 ft, the number of pulses N which can be delivered [Eq. (11)] is 201,250.

With a fixed mass system assumption, the propellant would last 2.415×10^7 sec, or 279.5 days [Eq. (13)]. However, with a variable mass system assumption, this propellant will provide only 265.5 days of fine control. Equation (14) is graphed in Fig. 1, which shows the relation in time for the same propellant consumption.

Using the same reference vehicle, the ratio of propellant consumption at the same control time can be shown as in Fig. 2. The significance of the discontinuity is that the propellant is completely expended under the variable mass conditions. It would thus require 85.2 lb of propellant for 279.5 days of attitude control. These relations can be used either for comparison purposes in this manner, or they can be solved to determine the amount of propellant required for a given control period.

It can be concluded from the preceding derivation and example that the significance of variable mass is dependent upon the operational conditions and the design characteristics of the vehicle. For small vehicles having propellant fractions in the range from 0.02 to 0.05, the additional propellant that can be calculated is negligible. In fact, as stated previously,

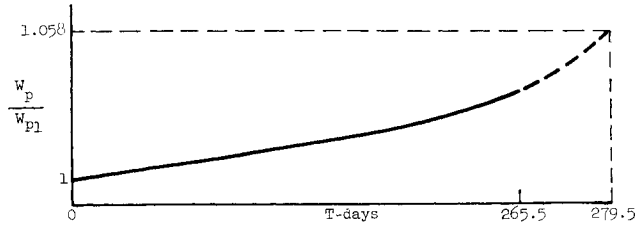

Fig. 2 Ratio of propellant weights vs time.

the additional propellant required due to system errors and external disturbing forces may far exceed this value. However, as the size of the vehicle, the length of the mission, or the propellant fraction is increased, the extra propellant required due to mass variance becomes more significant. The equations presented herein allow these propellant errors to be determined easily and thus they they can be considered in each individual design.

Reference

[1] Reeves, D. F., Boardman, W. P., and Baumann, H. A., "Pulsed rocket control techniques," ARS Paper 2704-62 (November 1962).

Application of Fiber Metals to the Meteoroid Protection Problem

FRANK J. ZIMMERMAN*
IIT Research Institute, Chicago, Ill.

A SERIES of meteoroid simulation impact experiments was conducted to determine the feasibility of using fiber metals as meteoroid shield materials. Fiber metals have many other properties that make them attractive for spacecraft applications such as strength, rigidity, and ability to withstand high temperatures and light weight. They are also similar in some respects to plastic foams that have been found to be quite effective in stopping simulated meteoroid particles.

Fiber metallurgy is centered around a basic process in which metal fibers are felted as in paper making and the felted fibers are sintered as in powder metallurgy. That is, randomly interlocked, felted fibers are heated to form a metallic weld bond at each point of contact between them. The sintered bodies may be further compacted, rolled, machined, welded, brazed, or treated in a variety of ways to fabricate finished, useful components having porosities of 5 to 97%. Some of the materials that have thus been treated are lead, aluminum, copper, iron, stainless steel, nickel, and cobalt-base alloys, titanium, and molybdenum. It appears that no metal or alloy is impossible to treat fiber-metallurgically, although those that form stable surface oxide films (e.g., aluminum) are more difficult to sinter. A schematic illustration of how one might utilize fiber metal panels is shown in Fig. 1.

Because fiber metal structural panels had already been made and studied and because such panels had been shown to be efficient absorbers of some types of energy, it was decided to evaluate the ability of the material to absorb the energy of impacting meteoroids. Assuming that fiber metal is found to be competitive with plastic fills to absorb meteoroid impact on a strength-to-weight basis, then the following additional advantages of fiber metal are also accrued: 1) higher service temperature than plastics; 2) use as load-bearing structures; 3) higher thermal conductivities, compared to plastics, make them more efficient thermal sinks; 4) greater resistance to space radiation damage; and 5) lower susceptibility to degradation by evaporation.

Since fiber metal materials possess strength characteristics roughly proportional to their density, the possibility exists for using them in thin sheets for spaced bumpers. In this application, they may be effective in breaking up the impacting particle and absorbing the residual particles on subsequent collisions. The goal of this series of impact experiments was to gain a better understanding of the performance of fiber metal materials and possibly formulate a physical model of their function in energy absorption.

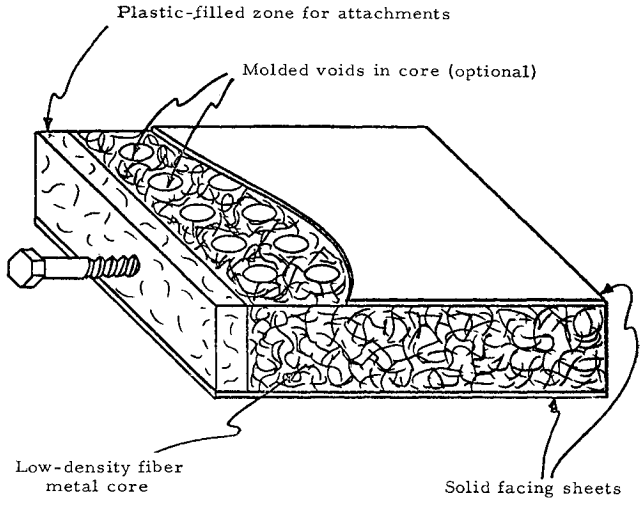

Fig. 1 Fiber-metal-core sandwich panel construction.

Several sets of hypervelocity impact experiments were conducted against fiber metal samples using the IITRI .22 caliber light gas gun. Simulated meteoroids ($\frac{1}{16}$-in. Pyrex spheres) weighing 4.54 mg were sabot-launched at velocities from 20,000 to 25,000 fps, and impact observations were made.

Fiber Metal Bumper Targets

In this series of firings, the targets were either thin, homogeneous metal sheets or fiber metal samples that were backed with an aluminum witness plate spaced 2 in. behind the primary target. Three sets of targets were used. In each set, a sheet of homogeneous materials was used as a control sample; then the varying relative densities of the same material in fiber metal form and the same area density were compared.

The first set used a control sample of 17-4 PH stainless steel, 0.031 in. thick, with an area density of 0.0176 psi. Three fiber metal samples of essentially the same area density, the same material, but with percentage densities of 64, 51, and 27 were then compared. It was found that as the percentage density of the fiber metal bumper decreased, the damage to the witness plate decreased accordingly. Penetration depth measurements were made on the witness plate to determine the greatest depth in all cases. Figure 2 shows that the maximum witness plate penetration generally follows a smooth curve as a function of percentage density.

The second set of targets made use of 1100 aluminum of the same area density as the stainless steel. A homogeneous control sample $\frac{3}{16}$ in. thick was used as were fiber metal samples of 51 and 30% density. It was found that the homogeneous aluminum in this thickness was sufficient to prevent damage to the witness plate even though the sheet suffered complete penetration. This demonstrates the relative efficiency of aluminum over stainless steel. The fiber metal samples completely stopped the projectiles without perforation and without any residual spray pattern.

Since the aluminum is a better bumper material than stainless steel from the weight standpoint, an additional aluminum series was fired using samples approximately one-half the area density. Control samples of two different types were used, one of 1100 and the other 7075 aluminum. The rest of this set included fiber metal samples of 1100 aluminum with relative densities of 60, 39, and 24%. The area densities were approximately the same as the control samples. A number of observations are possible: first, the

Presented at the AIAA Fifth Annual Structures and Materials Conference, Palm Springs, Calif., April 1–3, 1964 (no preprint number; published in bound volume of preprints of the meeting); revision received August 12, 1964.

* Manager, Ballistics and Explosives Research. Member AIAA.